Optical discovery of a relativistic jet from the tidal disruption of a star by a supermassive black hole

Igor Andreoni[1,2,3*†], Michael W. Coughlin[4†], Daniel A. Perley[5], Yuhan Yao[6], Wenbin Lu[7], S. Bradley Cenko[1,3], Harsh Kumar[8], Shreya Anand[9], Anna Y. Q. Ho[10,11,12], Mansi M. Kasliwal[6], Antonio de Ugarte Postigo[13,14], Steve Schulze[15], S. R. Kulkarni[6], Jesper Sollerman[16], Nial Tanvir[17], Armin Rest[18,19], Tomás Ahumada[2], G. C. Anupama[20], Katie Auchettl[21,22,23], Sudhanshu Barway[20], Varun Bhalerao[8], Joshua S. Bloom[24,11], Mattia Bulla[16], Eric Burns[25], Sergio Campana[26], Panos Charalampopoulos[27], Jeff Cooke[28,29], Valerio D'Elia[30], Kaustav Kashyap Das[9], Dougal Dobie[28,29], José Feliciano Agüí Fernández[13], James Freeburn[28,29], Cristoffer Fremling[6], Suvi Gezari[18], Matthew Graham[6], Erica Hammerstein[2], Luca Izzo[31], D. Alexander Kann[13], David L. Kaplan[32], Viraj R. Karambelkar[9], Erik C. Kool[16], Giorgos Leloudas[27], Andrew Levan[33], Michael J. Lundquist[34], M. Coleman Miller[1,2], Anais Möller[35], Emmy Paraskeva[36,37,38,39], Miika Pursiainen[40], Vikram Ravi[9], Ryan Ridden-Harper[41,42], Antonio C. Rodriguez[6], Ana Saguès-Carrecedo[15], I. A. Smith[43], Jean J. Somalwar[9], Christina Thöne[13], Frank Valdes[44], Jan van Roestel[6], Susanna D. Vergani[45,46], Qinan Wang[18], Jielai Zhang[28,29] [affiliations can be found after the references]

Stars approaching supermassive black holes (SMBHs) at the center of galaxies can be disrupted by tidal forces and illuminate the electromagnetic spectrum. Space-based observatories performing searches in γ-rays and X-rays have unveiled a handful with relativistic jets, the last one more than a decade ago. Here we report the optical discovery of AT2022cmc a transient source located at a redshift $z = 1.19335$. The discovery of a very bright counterpart at other wavelengths, including in X-rays, sub-millimeter, and radio, supports the interpretation of AT2022cmc as a jetted tidal disruption event (TDE) containing a synchrotron "afterglow". Optical and ultraviolet observations revealed a fast-fading red "flare" (~ 1 day) soon dominated by a slow blue "plateau", hence enabling the study of two components generated by the tidal disruption: the relativistic jet and the optically thick outflows from the self-crossing shock and the accretion disk. [A SENTENCE ON RATES WHEN AVAILABLE]. Forthcoming optical surveys have the potential to unveil a population of transients of the AT2022cmc class.

On 2022 February 11 10:42:40 UTC the Zwicky Transient Facility (ZTF[1]), in its nightly cadenced survey[CIT], detected a transient, ZTF22aaajecp (Fig. 1), located at J2000 right ascension

[*] Neil Gehrels Fellow.
[†] These two authors contributed equally to this work.

α = $13^{\mathrm{h}}34^{\mathrm{m}}43.201^{\mathrm{s}}$ and declination δ = $+33°13'00.648''$.[a] A pipeline called "ZTFReST"[2], using data obtained on the next two nights, flagged it to be of high value due to its rapid rise and fade. ZTFReST is designed for enabling real-time discovery of elusive transients including compact binary merger products (known as kilonovae[3]) in optical survey data, which require online frameworks to enable successful identification and follow-up observations.

We registered the source with the Transient Name Server (TNS)[b] which then assigned[4] the IAU name AT2022cmc. A bright X–ray counterpart was found[5] with a 0.3–6 keV flux of $(3.04{\pm}0.05){\times}10^{-11}$ erg s^{-1}cm^{-2} (Supplementary Information sec. 4.0.11-4.0.12), as well as in the decimetric[6] and in the sub-millimeter[7] bands (Fig. 2; Supplementary Information sec. 4.0.4-4.0.5). The redshift of the host galaxy, $z = 1.19335 \pm 0.00021$, was secured by absorption and emission lines in the spectrum obtained with the European Southern Observatory's X-shooter instrument[8] (Fig. 3; Supplementary Information sec. 4.0.13).

We undertook an intensive multi-wavelength monitoring program. The infrared/optical/ultraviolet light curve (Fig. 1) showed a red color and rapid rise and decay for about two days (rest frame) post-discovery, before the evolution slowed and the color became bluer. Observations with the Very Large Array (VLA), the Submillimeter Array (SMA), and JCMT SCUBA-2 Sub-millimetre, which started on 2022 February 15 12:06 UT, showed that the radio spectrum was self-absorbed up to hundreds of GHz. The X–ray, radio, and submillimeter counterparts are all among the most luminous identified to date for cosmological transients (see Supplementary Material).

Interpretation

The exceptionally high luminosity and rapid spectral and temporal evolution mark AT2022cmc as an extremely unusual transient, even amongst the rapidly expanding "zoo" of objects that now populate almost every region of the parameter space (Fig.1). Of the known classes of transient sources, we consider four potential models as viable because of the fast optical variability and the existence of radio and X–ray counterparts: a γ-ray burst arising due to the collapse of a star (GRB), a kilonova arising from r-process element production in a compact binary merger, a fast blue optical transient (FBOT[9,10]), which are not well-understood but are likely related to stellar

[a] These coordinates were obtained from Hubble Space Telescope follow-up images.

[b] `https://www.wis-tns.org/`

collapse to a black hole, and a jetted tidal disruption event (TDE) scenario, where a supermassive black hole accretes matter from a star.

The observed redshift of AT2022cmc implies that the intrinsic optical isotropic equivalent luminosity is comparable only to the brightest relativistic transients (Fig. 2, left panel). Such a high luminosity ($M \approx -25$ mag in r-band) along with the red color at peak and rapid decline, are consistent with synchrotron emission; this behavior is usually observed in cosmological afterglows associated with GRBs, some of which were discovered in ZTF data by ZTFReST[2] and other fast transient filtering algorithms[11,12]. Optical GRB afterglows are typically characterized by a short ($\sim$ seconds to minutes) rise phase, with rare exceptions [13], so the early ZTF faint detections in both r- and g-band of AT2022cmc (11.6 minutes from each other and 10.8 hours before the brightest optical data point) suggest that the rise time was likely longer than typical for an on-axis afterglow. The large X–ray and radio isotropic equivalent luminosity and fast variability[CIT Pasham's ATel] separate AT2022cmc from the class of GRB afterglows (Fig. 2, right panel) and is in contrast with an off-axis GRB interpretation (however see [14]). A blue slow component at late time is not predicted for GRB afterglows.

The red color and rapid evolution of AT2022cmc recall the behavior of the optical/infrared kilonova AT2017gfo[15] associated with GW170817[16], the first binary neutron star merger detected in gravitational waves. The luminosity of kilonovae is however orders of magnitude lower than most extragalactic transients (GW170817 was $M \sim -16.5$ mag at peak), even when models with high ejecta mass are invoked, and those models evolve from blue to red (whereas AT2022cmc is red to blue).

A recently discovered class of sources known as fast blue optical transients (FBOTs[9,10]) exhibit observer-frame light curves that look similar to AT2022cmc. Similarly to AT2022cmc, FBOTs have bright X–ray and radio counterparts[12,17–19]. At early phases, the optical light curve of AT2022cmc fades $\sim 2\times$ faster than the prototypical FBOT, AT2018cow, it is much redder, and $> 83\times$ brighter in r-band at peak. A long-duration blue component has not been observed in FBOTs to date. Altogether these properties exclude this scenario.

The luminosity of the X–ray and the submillimiter counterparts to AT2022cmc are comparable to only the most luminous GRB afterglows and to the relativistic tidal disruption event (TDE), Swift J1644+57[20–23]. Swift J1644+57 was first detected as a GRB, but its follow-up revealed exceptional characteristics that is most commonly explained by relativistic emission from the tidal disruption of a star by a supermassive black hole. A near-infrared transient was detected associated with Swift J1644+57, which faded beyond the detection limit in $\sim\ 10\,\mathrm{days}$[21]. No optical or ultraviolet transient was detected[21,22], probably because it was suppressed by the host galaxy dust extinction, which was estimated to be $A_V \approx 4.5$ (corresponding to a neutral hydrogen column density of NH$\approx\ 1 \times 10^{22}\,\mathrm{cm}^{-2}$)[21]. From the Swift/XRT data analysis of AT2022cmc (see Methods), we estimate that the neutral hydrogen column density of the host galaxy is NH$<$ $6.4\times10^{21}\,\mathrm{cm}^{-2}$ (90% confidence). The presence of a counterpart in the ultraviolet, first detected by the Neil Gehrels Swift Observatory on 2022 February 23 (day 5.334) with magnitude $UWM2 = (21.30 \pm 0.25)$ mag, suggests that the host galaxy extinction is significantly lower than in the case of Swift J1644+57.

We conclude that AT2022cmc is most likely generated by jetted material from the tidal disruption of a star by a massive black hole at the center of a galaxy with low dust extinction. Two more jetted TDE candidates have been detected by Swift with similar X-ray and radio properties: Swift J2058+05 [24,25] and Swift J1112-82 [26], which implied a rate of jetted TDEs of $\approx 3\times10^{-10} yr^{-1}$ per galaxy, likely because only ~10% of TDEs produce relativistic jets, and of those that do, they typically have a small beaming angle $\sim 1\,\mathrm{deg}$)[26]. [TO DO, Jean, Ana are working on rates; add implications for high energy particles].

We now describe a possible explanation for AT2022cmc, aided by the broad-brush picture shown in Fig. 4. The event started when a ill-fated star approached the black hole on a nearly parabolic trajectory and was tidally crushed and stretched into a long stream of debris gas. About half of the mass stays bound to the black hole, undergoes general relativistic apsidal precession as the gas falls back towards the pericenter, and then produces strong shocks at the self-crossing point [27–30]. The shocked gas then circularizes to form an accretion disk around the black hole whose rapid spin generates a pair of relativistic jets [31]. The high X-ray luminosity and hour timescale flux variability suggest that the X-rays are generated by internal dissipation within the jet at a distance less than $10^{16}\,\mathrm{cm}$ ($\sim$ 0.01 pc) from the black hole and that our line of sight is within the one of the jets' relativistic beaming cone, as was also the case for Swift J1644+57.

The fast-fading red component can be explained as follows. As the jet, which carries 10^{52}–$10^{53}\,\mathrm{erg}$

of energy, propagates to large distances of $r \sim 0.1\,\mathrm{pc}$, it is significantly decelerated by driving a forward shock into the surrounding gas and a reverse shock propagating into the jet material, similar to cosmological gamma-ray bursts [32]. Electrons are accelerated to relativistic speeds by these shocks and then produce synchrotron emission in the radio/millimeter-bands up to optical wavelengths. The non-thermal optical emission from the synchrotron afterglow is expected to have a variability timescale of $r/(2\Gamma^2 c) \sim 0.6\,\mathrm{day}\,(\mathrm{r}/0.1\,\mathrm{pc})(\Gamma/10)^{-2}$, where Γ is the Lorentz factor of the emitting gas and c is the speed of light.

Another source of thermal optical/UV emission is the optically thick outflows from the self-crossing shock and the accretion disk [30,33,34], which can be responsible for the blue plateau observed for weeks after the initial flare. As is known from non-jetted TDEs, this gas component produces a blackbody-like spectrum with temperature $\gtrsim 3{\times}10^4\,\mathrm{K}$ and luminosity of 10^{44}–$10^{45}\,\mathrm{erg/s}$, consisting with our optical obervations at peak. This luminosity varies on the gas expansion timescale of $r_{\rm ph}/v \sim 10\,\mathrm{day}\,(r_{\rm ph}/10^{15}\,\mathrm{cm})(v/10^9\,\mathrm{cm\,s^{-1}})^{-1}$, where $r_{\rm ph}$ is the photospheric radius and v is the outflow speed.

The growth of astronomy facilities and their associated data sets across wavelengths and messengers, such as Advanced LIGO[35] and Advanced Virgo[36] for gravitational waves, IceCube[37] and ANTARES[38] for neutrinos, and ZTF[1] and the forthcoming Vera C. Rubin Observatory[39] are transforming astrophysics with detections of never-before-seen phenomena like AT2022cmc. The discovery of energetic phenomena that were the exclusive dominion of gamma–ray and X–ray observatories have become accessible to the optical community in particular via systematic, high-cadence, wide-field observations. Using AT2022cmc's light curve and the ZTF survey footprint so far, this detection implies an intrinsic rate of $?^{+?}_{-?}\,\mathrm{Mpc^{-3}\,yr^{-1}}$, opening the door to many more in the Rubin era, when we will use them to understand the dynamics of the jets, why some TDEs produce relativistic jets and others do not, and whether jetted TDEs are multi-messenger sources of neutrinos and cosmic rays.

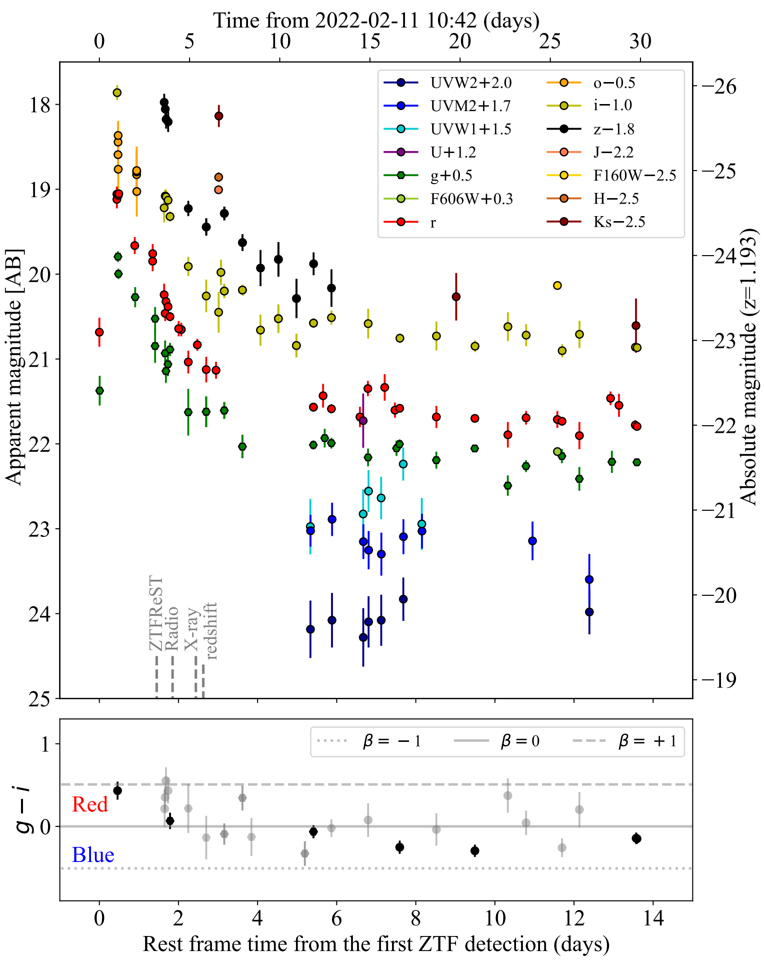

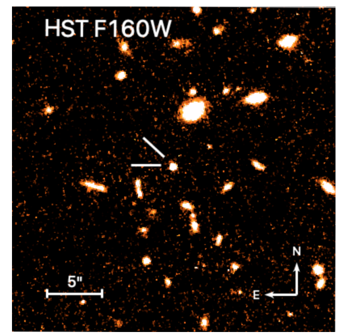

(b) Hubble Space Telescope image

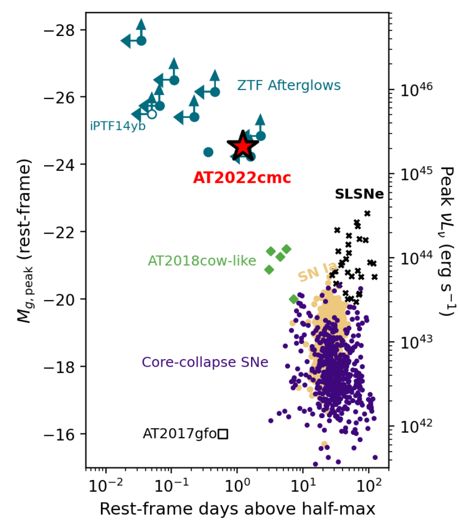

(a) nIR/optical/UV light curve

(c) Optical transient parameter space

Figure 1: **AT2022cmc in the near infrared, optical, and ultraviolet.** Apparent and absolute magnitudes are plotted in (a), showing the fast evolution and the large luminosity of the transient in the optical. In the bottom panel, β is the spectral index defined as $f_\nu \sim \nu^\beta$, which means $\beta = (m_i - m_g)/2.5/\log_{10}(\lambda_i/\lambda_g)$ where $\lambda_i = 7458$ Åand $\lambda_g = 4672$ Åare the effective wavelengths; data points with S/N> 10 are colored in black, the others in grey. AT2022cmc was clearly detected in HST images (b) in $F160W$ and $F606W$ filters, which also revealed an overdensity of red galaxies within $\sim 20''$ from the transient location. The luminosity and evolution timescale of AT2022cmc separates it from most classes of optical transients[40] (c).

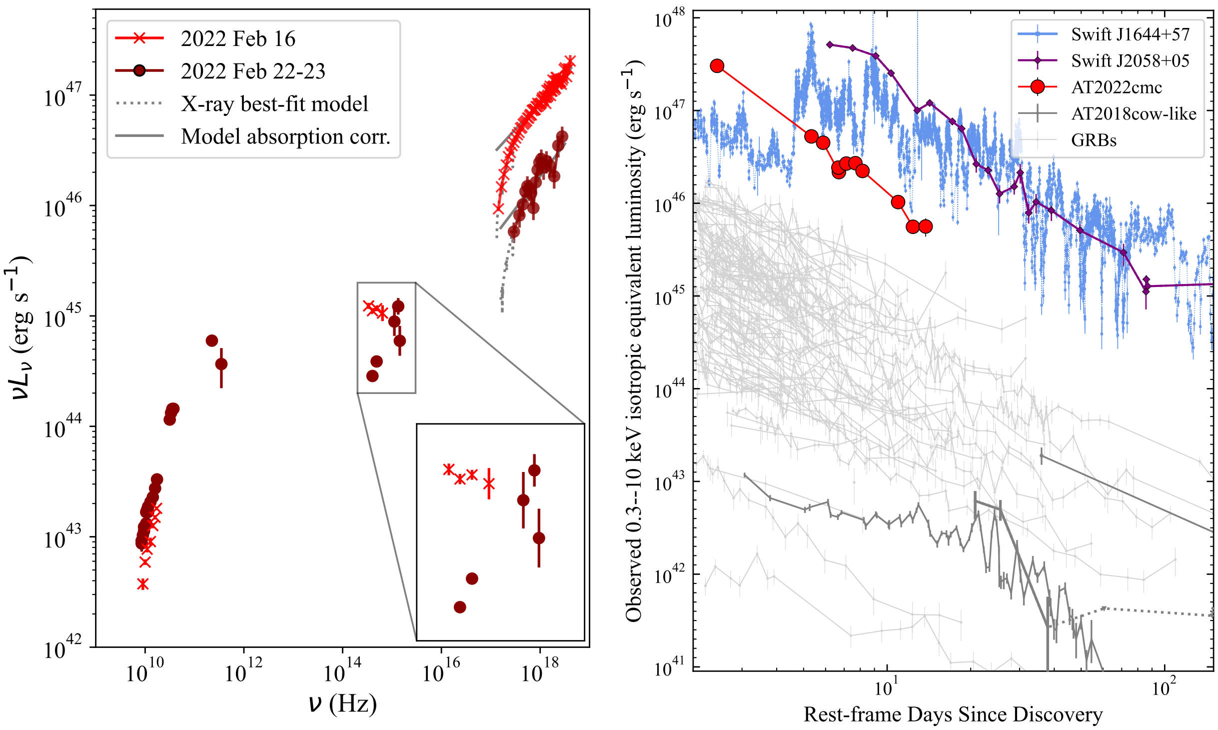

Figure 2: **Multi-wavelength isotropic equivalent luminosity of AT2022cmc.** *Left* – SED of AT2022cmc including radio (VLA), millimiter (SMA, ...), optical (LT, ...), UV (Swift/UVOT), and X–ray (Swift/XRT, NICER [to be updated]) data. A rapid change in the shape of the SED is especially evident in the optical/UV between $\sim 2.5\,$d and $\sim 6\,$d in the rest frame from the first detection. *Right* –The isotropic equivalent luminosity of AT2022cmc surpasses all Swift long GRB afterglows with measured redshifts (in lightgrey), in the 0.3–10 keV energy range, by at least one order of magnitude. It is also larger than AT2018cow-like transients (in darkgrey) and comparable only to jetted TDEs such as Swift J1644+57[41] and Swift J2058+05[25]. We caution that the onset time of AT2022cmc might have happened hours or even days before the first ZTF detection, which would make the XRT light curve shift rightward in the plot.

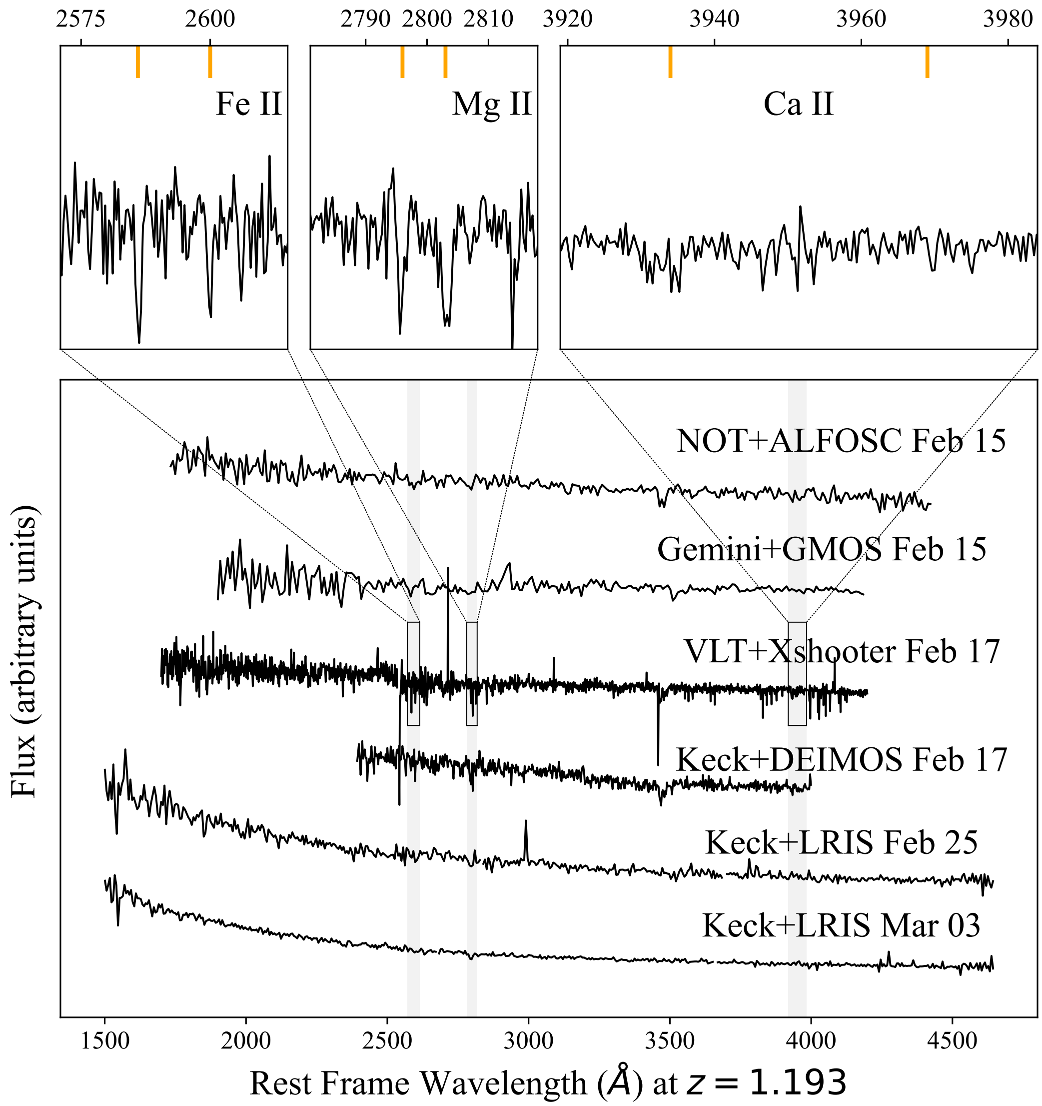

Figure 3: **Spectra at rest frame for redshift z=1.193.** Optical spectra were acquired from the night after the identification of AT2022cmc until several weeks afterwards. Absorption lines in the VLT/X-shooter spectrum (top panels) enabled the redshift to be established. In the first two weeks since its first detection, the spectra of AT2022cmc appear otherwise featureless. The absorption line around 3,500Åis telluric (non astrophysical) and the narrow emission lines were deemed cosmic rays.

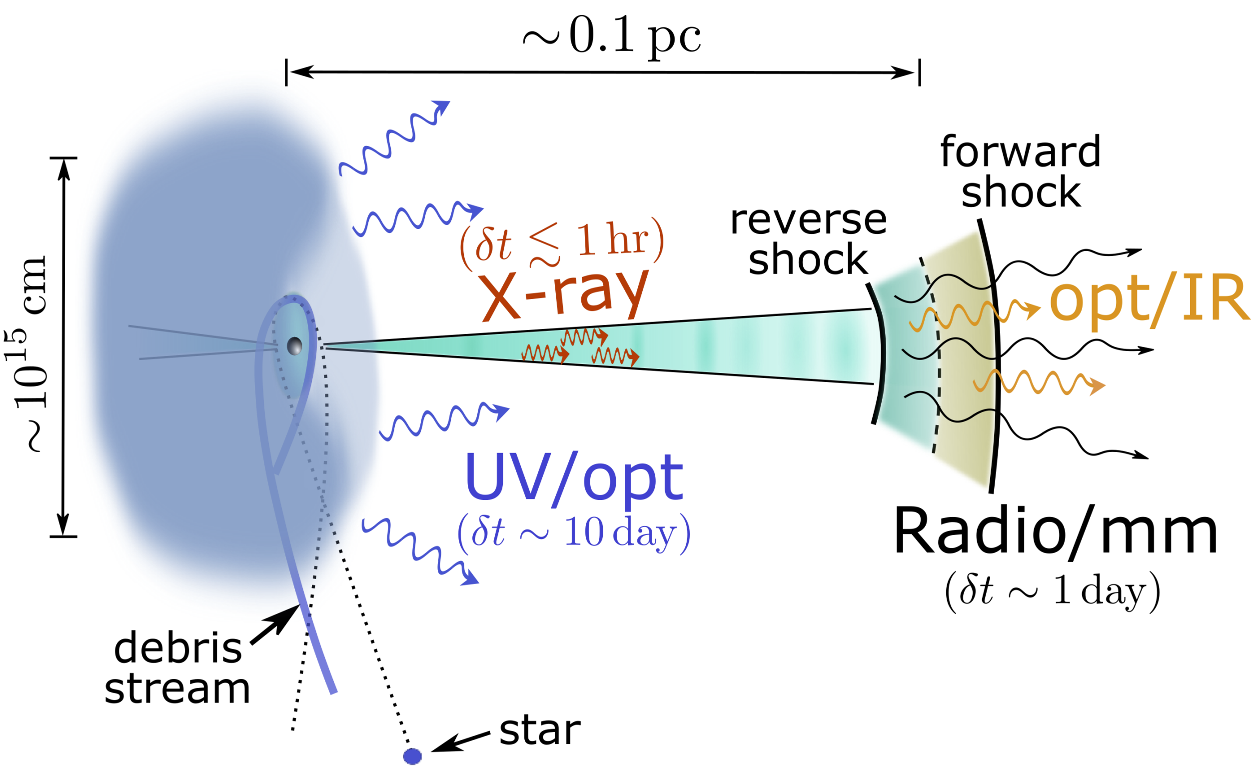

Figure 4: **Sketch**. Black dotted line: original geodesic of the star (note the GR apsidal precession). Thick blue line: debris gas of the disrupted star (note the self-intersection). Thick blue torus ($\sim$1e15cm): optically thick gas reprocessing the disk X-rays into the UV/optical band (as observed from other non-jetted TDEs). Light blue disk ($\sim$ tidal disruption radius $\sim$ 1e13cm): accretion disk near the SMBH. Jets: color fluctuations indicate that the jet power is unsteady (as suggested by rapid X–ray variability). External shocks ($\sim$0.1 pc): reverse shock dominates the radio/millimeter emission, and both reverse shock and forward shock contribute to the non-thermal optical/IR. δt for each component indicates the typical evolution timescale.

1. Bellm, E. C. *et al.* The Zwicky Transient Facility: System Overview, Performance, and First Results. PASP **131**, 018002 (2019). 1902.01932.

2. Andreoni, I. *et al.* Fast-transient Searches in Real Time with ZTFReST: Identification of Three Optically Discovered Gamma-Ray Burst Afterglows and New Constraints on the Kilonova Rate. ApJ **918**, 63 (2021). 2104.06352.

3. Metzger, B. D. Kilonovae. *Living Reviews in Relativity* **23**, 1 (2019). 1910.01617.

4. Andreoni, I. ZTF Transient Discovery Report for 2022-02-14. *Transient Name Server Discovery Report* **2022-397**, 1 (2022).

5. Pasham, D., Gendreau, K., Arzoumanian, Z. & Cenko, B. ZTF22aaajecp/AT2022cmc: NICER X-ray detection. *GRB Coordinates Network* **31601**, 1 (2022).

6. Perley, D. A. ZTF22aaajecp/AT2022cmc: VLA radio detection. *GRB Coordinates Network* **31592**, 1 (2022).

7. Perley, D. A., Ho, A. Y. Q., Petitpas, G. & Keating, G. ZTF22aaajecb/AT2022cmc: Submillimeter Array detection. *GRB Coordinates Network* **31627**, 1 (2022).

8. Tanvir, N. R. *et al.* ZTF22aaajecp/AT2022cmc: VLT/X-shooter redshift. *GRB Coordinates Network* **31602**, 1 (2022).

9. Drout, M. R. *et al.* Rapidly Evolving and Luminous Transients from Pan-STARRS1. ApJ **794**, 23 (2014). 1405.3668.

10. Perley, D. A. *et al.* The fast, luminous ultraviolet transient AT2018cow: extreme supernova, or disruption of a star by an intermediate-mass black hole? MNRAS **484**, 1031–1049 (2019). 1808.00969.

11. Ho, A. Y. Q. *et al.* ZTF20aajnksq (AT 2020blt): A Fast Optical Transient at z = 2.9 with No Detected Gamma-Ray Burst Counterpart. ApJ **905**, 98 (2020). 2006.10761.

12. Ho, A. Y. Q. *et al.* Luminous Millimeter, Radio, and X-ray Emission from ZTF20acigmel (AT2020xnd). *arXiv e-prints* arXiv:2110.05490 (2021). 2110.05490.

13. Djorgovski, S. G. *et al.* The optical counterpart to the gamma-ray burst GRB970508. Nature **387**, 876–878 (1997).

14. Quataert, E. & Kasen, D. Swift 1644+57: the longest gamma-ray burst? MNRAS **419**, L1–L5 (2012). 1105.3209.

15. Coulter et al. Swope supernova survey 2017a (sss17a), the optical counterpart to a gravitational wave source. *Science* **358**, 1556–1558 (2017).

16. Abbott et al. Gw170817: Observation of gravitational waves from a binary neutron star inspiral. *Phys. Rev. Lett.* **119**, 161101 (2017). URL https://link.aps.org/doi/10.1103/PhysRevLett.119.161101.

17. Ho, A. Y. Q. *et al.* AT2018cow: A Luminous Millimeter Transient. ApJ **871**, 73 (2019). 1810.10880.

18. Margutti, R. *et al.* An Embedded X-Ray Source Shines through the Aspherical AT 2018cow: Revealing the Inner Workings of the Most Luminous Fast-evolving Optical Transients. ApJ **872**, 18 (2019). 1810.10720.

19. Yao, Y. *et al.* The X-ray and Radio Loud Fast Blue Optical Transient AT2020mrf: Implications for an Emerging Class of Engine-Driven Massive Star Explosions. *arXiv e-prints* arXiv:2112.00751 (2021). 2112.00751.

20. Bloom, J. S. *et al.* A Possible Relativistic Jetted Outburst from a Massive Black Hole Fed by a Tidally Disrupted Star. *Science* **333**, 203 (2011). 1104.3257.

21. Burrows, D. N. *et al.* Relativistic jet activity from the tidal disruption of a star by a massive black hole. Nature **476**, 421–424 (2011). 1104.4787.

22. Levan, A. J. *et al.* An Extremely Luminous Panchromatic Outburst from the Nucleus of a Distant Galaxy. *Science* **333**, 199 (2011). 1104.3356.

23. Zauderer, B. A. *et al.* Birth of a relativistic outflow in the unusual gamma-ray transient Swift J164449.3+573451. Nature **476**, 425–428 (2011). 1106.3568.

24. Cenko, S. B. *et al.* Swift J2058.4+0516: Discovery of a Possible Second Relativistic Tidal Disruption Flare? ApJ **753**, 77 (2012). 1107.5307.

25. Pasham, D. R. *et al.* A Multiwavelength Study of the Relativistic Tidal Disruption Candidate Swift J2058.4+0516 at Late Times. ApJ **805**, 68 (2015). 1502.01345.

26. Brown, G. C. *et al.* Swift J1112.2-8238: a candidate relativistic tidal disruption flare. MNRAS **452**, 4297–4306 (2015). 1507.03582.

27. Shiokawa, H., Krolik, J. H., Cheng, R. M., Piran, T. & Noble, S. C. General Relativistic Hydrodynamic Simulation of Accretion Flow from a Stellar Tidal Disruption. ApJ **804**, 85 (2015). 1501.04365.

28. Hayasaki, K., Stone, N. & Loeb, A. Circularization of tidally disrupted stars around spinning supermassive black holes. MNRAS **461**, 3760–3780 (2016). 1501.05207.

29. Bonnerot, C., Rossi, E. M., Lodato, G. & Price, D. J. Disc formation from tidal disruptions of stars on eccentric orbits by Schwarzschild black holes. MNRAS **455**, 2253–2266 (2016). 1501.04635.

30. Lu, W. & Bonnerot, C. Self-intersection of the fallback stream in tidal disruption events. MNRAS **492**, 686–707 (2020). 1904.12018.

31. Blandford, R. D. & Znajek, R. L. Electromagnetic extraction of energy from Kerr black holes. MNRAS **179**, 433–456 (1977).

32. Kumar, P. & Zhang, B. The physics of gamma-ray bursts & relativistic jets. Phys. Rep. **561**, 1–109 (2015). 1410.0679.

33. Strubbe, L. E. & Quataert, E. Optical flares from the tidal disruption of stars by massive black holes. MNRAS **400**, 2070–2084 (2009). 0905.3735.

34. Metzger, B. D. & Stone, N. C. A bright year for tidal disruptions. MNRAS **461**, 948–966 (2016). 1506.03453.

35. Aasi et al. Advanced ligo. *Classical and Quantum Gravity* **32**, 074001 (2015).

36. Acernese et al. Advanced Virgo. *Classical and Quantum Gravity* **32**, 024001 (2015).

37. Aartsen, M. *et al.* The IceCube neutrino observatory: instrumentation and online systems. *Journal of Instrumentation* **12**, P03012–P03012 (2017). URL https://doi.org/10.1088%2F1748-0221%2F12%2F03%2Fp03012.

38. Ageron, M. *et al.* Antares: The first undersea neutrino telescope. *Nuclear Instruments and Methods in Physics Research Section A: Accelerators, Spectrometers, Detectors and*

Associated Equipment **656**, 11–38 (2011). URL `https://www.sciencedirect.com/science/article/pii/S0168900211013994`.

39. Ivezić, Ž. *et al.* LSST: From Science Drivers to Reference Design and Anticipated Data Products. ApJ **873**, 111 (2019). `0805.2366`.

40. Ho, A. Y. Q. *et al.* Cosmological Fast Optical Transients with the Zwicky Transient Facility: A Search for Dirty Fireballs. *arXiv e-prints* arXiv:2201.12366 (2022). `2201.12366`.

41. Mangano, V., Burrows, D. N., Sbarufatti, B. & Cannizzo, J. K. The Definitive X-Ray Light Curve of Swift J164449.3+573451. ApJ **817**, 103 (2016). `1511.06447`.

42. Flaugher, B. *et al.* The Dark Energy Camera. AJ **150**, 150 (2015). `1504.02900`.

43. Valdes, F., Gruendl, R. & DES Project. The DECam Community Pipeline. In Manset, N. & Forshay, P. (eds.) *Astronomical Data Analysis Software and Systems XXIII*, vol. 485 of *Astronomical Society of the Pacific Conference Series*, 379 (2014).

44. Rest, A. *et al.* Cosmological Constraints from Measurements of Type Ia Supernovae Discovered during the First 1.5 yr of the Pan-STARRS1 Survey. ApJ **795**, 44 (2014). `1310.3828`.

45. Gendreau, K. C. *et al.* The Neutron star Interior Composition Explorer (NICER): design and development. In *Space Telescopes and Instrumentation 2016: Ultraviolet to Gamma Ray*, vol. 9905 of *Society of Photo-Optical Instrumentation Engineers (SPIE) Conference Series*, 99051H (2016).

46. Remillard, R. A. *et al.* An Empirical Background Model for the NICER X-Ray Timing Instrument. AJ **163**, 130 (2022). `2105.09901`.

47. HI4PI Collaboration *et al.* HI4PI: A full-sky H I survey based on EBHIS and GASS. A&A **594**, A116 (2016). `1610.06175`.

48. Burrows, D. N. *et al.* The Swift X-Ray Telescope. Space Sci. Rev. **120**, 165–195 (2005). `astro-ph/0508071`.

49. Roming, P. W. A. *et al.* The Swift Ultra-Violet/Optical Telescope. Space Sci. Rev. **120**, 95–142 (2005). `astro-ph/0507413`.

50. Cash, W. Parameter estimation in astronomy through application of the likelihood ratio. ApJ **228**, 939–947 (1979).

51. Tonry, J. L. *et al.* ATLAS: A High-cadence All-sky Survey System. PASP **130**, 064505 (2018). 1802.00879.

52. Smith, K. W. *et al.* Design and Operation of the ATLAS Transient Science Server. PASP **132**, 085002 (2020). 2003.09052.

53. Johnson, B. D., Leja, J., Conroy, C. & Speagle, J. S. Stellar Population Inference with Prospector. ApJS **254**, 22 (2021). 2012.01426.

54. Conroy, C., Gunn, J. E. & White, M. The Propagation of Uncertainties in Stellar Population Synthesis Modeling. I. The Relevance of Uncertain Aspects of Stellar Evolution and the Initial Mass Function to the Derived Physical Properties of Galaxies. ApJ **699**, 486–506 (2009). 0809.4261.

55. Foreman-Mackey, D., Sick, J. & Johnson, B. Python-Fsps: Python Bindings To Fsps (V0.1.1) (2014).

56. Byler, N., Dalcanton, J. J., Conroy, C. & Johnson, B. D. Nebular Continuum and Line Emission in Stellar Population Synthesis Models. ApJ **840**, 44 (2017). 1611.08305.

57. Chabrier, G. Galactic Stellar and Substellar Initial Mass Function. PASP **115**, 763 (2003). astro-ph/0304382.

58. Calzetti, D. *et al.* The Dust Content and Opacity of Actively Star-forming Galaxies. ApJ **533**, 682–695 (2000). astro-ph/9911459.

59. Schulze, S. *et al.* The Palomar Transient Factory Core-collapse Supernova Host-galaxy Sample. I. Host-galaxy Distribution Functions and Environment Dependence of Core-collapse Supernovae. ApJS **255**, 29 (2021). 2008.05988.

[1]*Joint Space-Science Institute, University of Maryland, College Park, MD 20742, USA*

[2]*Department of Astronomy, University of Maryland, College Park, MD 20742, USA*

[3]*Astrophysics Science Division, NASA Goddard Space Flight Center, Mail Code 661, Greenbelt, MD 20771, USA*

[4]School of Physics and Astronomy, University of Minnesota, Minneapolis, Minnesota 55455, USA
[5]Astrophysics Research Institute, Liverpool John Moores University, IC2, Liverpool Science Park, 146 Brownlow Hill, Liverpool L3 5RF, UK
[6]Division of Physics, Mathematics and Astronomy, California Institute of Technology, Pasadena, CA 91125, USA
[7]Department of Astrophysical Sciences, Princeton University, Princeton, NJ 08544, USA
[8]Indian Institute of Technology Bombay, Powai, Mumbai 400076, India
[9]Division of Physics, Mathematics, and Astronomy, California Institute of Technology, Pasadena, CA 91125, USA
[10]Department of Astronomy, University of California, Berkeley, CA 94720-3411, USA
[11]Lawrence Berkeley National Laboratory, 1 Cyclotron Road, MS 50B-4206, Berkeley, CA 94720, USA
[12]Miller Institute for Basic Research in Science, 468 Donner Lab, Berkeley, CA 94720, USA
[13]Instituto de Astrofísica de Andalucía, Glorieta de la Astronomía,E-18008, Granada, Spain
[14]Artemis, Observatoire de la Côte d'Azur, Université Côte d'Azur, Boulevard de l'Observatoire, 06304 Nice, France
[15]The Oskar Klein Centre, Department of Physics, Stockholm University, AlbaNova, SE-106 91 Stockholm, Sweden
[16]The Oskar Klein Centre, Department of Astronomy, Stockholm University, AlbaNova, SE-106 91 Stockholm, Sweden
[17]Department of Physics and Astronomy, University of Leicester, University Road, LE1 7RH, U.K
[18]Space Telescope Science Institute, 3700 San Martin Drive, Baltimore, MD 21218, USA
[19]Department of Physics and Astronomy, The Johns Hopkins University, 3400 North Charles Street, Baltimore, MD 21218, USA
[20]Indian Institute of Astrophysics, Bangalore 560034, India
[21]School of Physics, University of Melbourne, Parkville, Victoria 3010, Australia
[22]ARC Centre of Excellence for All Sky Astrophysics in 3 Dimensions (ASTRO 3D)
[23]Department of Astronomy and Astrophysics, University of California, Santa Cruz, CA 95064, USA
[24]Department of Astronomy, University of California, Berkeley, CA 94720, USA
[25]Department of Physics & Astronomy, Louisiana State University, Baton Rouge, LA 70803, USA
[26]INAF-Osservatorio Astronomico di Brera, Via E. Bianchi 46, I-23807 Merate (LC), Italy
[27]DTU Space, National Space Institute, Technical University of Denmark, Elektrovej 327, 2800 Kgs. Lyngby, Denmark
[28]Australian Research Council Centre of Excellence for Gravitational Wave Discovery (OzGrav), Swinburne University of Technology, Hawthorn, VIC, 3122, Australia
[29]Centre for Astrophysics and Supercomputing, Swinburne University of Technology, Hawthorn, VIC,

3122, Australia

[30]Space Science Data Center - Agenzia Spaziale Italiana, via del Politecnico, s.n.c., I-00133, Roma, Italy

[31]DARK, Niels Bohr Institute, University of Copenhagen, Jagtvej 128, 2200 Copenhagen

[32]Center for Gravitation, Cosmology and Astrophysics, Department of Physics, University of Wisconsin–Milwaukee, P.O. Box 413, Milwaukee, WI 53201, USA

[33]Department of Astrophysics, Radboud University, 6525 AJ Nijmegen, The Netherlands

[34]W. M. Keck Observatory, 65-1120 Mamalahoa Highway, Kamuela, HI 96743, USA

[35]Swinburne University of Technology, Hawthorn, VIC, 3122, Australia

[36]IAASARS, National Observatory of Athens, 15236, Penteli, Greece

[37]Department of Astrophysics, Astronomy & Mechanics, Faculty of Physics, National and Kapodistrian University of Athens, 15784, Athens, Greece

[38]Nordic Optical Telescope, Rambla Jose Ana Fernandez Perez, 7, 38711 Brena Baja, Spain

[39]Department of Physics and Astronomy, Aarhus University, NyMunkegade 120, DK-8000 Aarhus C, Denmark

[40]DTU Space, National Space Institute, Technical University of Denmark, Elektrovej 327, DK-2800 Kgs. Lyngby, Denmark

[41]School of Physical and Chemical Sciences — Te Kura Matu, University of Canterbury, Private Bag 4800, Christchurch 8140, New Zealand

[42]Department of Physics and Astronomy, The Johns Hopkins University, Baltimore, MD 21218, USA

[43]Institute for Astronomy, University of Hawaii, 2680 Woodlawn Drive, Honolulu, HI 96822

[44]National Optical Astronomy Observatory, P.O. Box 26732, Tucson, AZ 85719, USA

[45]GEPI, Observatoire de Paris, PSL Research University, CNRS, Place Jules Janssen, 92190 Meudon

[46]Institut d'Astrophysique de Paris, CNRS-UPMC, UMR7095, 98bis bd Arago, 75014 Paris, France

Acknowledgements The authors thank Dheeraj R. Pasham and Sam Oates.

Based on observations obtained with the Samuel Oschin Telescope 48-inch and the 60-inch Telescope at the Palomar Observatory as part of the Zwicky Transient Facility project. ZTF is supported by the National Science Foundation under Grant No. AST-1440341 and a collaboration including Caltech, IPAC, the Weizmann Institute for Science, the Oskar Klein Center at Stockholm University, the University of Maryland, the University of Washington (UW), Deutsches Elektronen-Synchrotron and Humboldt University, Los Alamos National Laboratories, the TANGO Consortium of Taiwan, the University of Wisconsin at Milwaukee, and Lawrence Berkeley National Laboratories. Operations are conducted by Caltech Optical Observatories, IPAC, and UW. The work is partly based on the observations made with the Gran Telescopio Canarias (GTC), installed in the Spanish Observatorio del Roque de los Muchachos of the Instituto de

Astrofisica de Canarias, in the island of La Palma. One of us also acknowledges all co-Is of our GTC proposal. SED Machine is based upon work supported by the National Science Foundation under Grant No. 1106171. The ZTF forced-photometry service was funded under the Heising-Simons Foundation grant #12540303 (PI: Graham).

M. W. Coughlin acknowledges support from the National Science Foundation with grant numbers PHY-2010970 and OAC-2117997. E. C. Kool acknowledges support from the G.R.E.A.T research environment and the Wenner-Gren Foundations. H. Kumar thanks the LSSTC Data Science Fellowship Program, which is funded by LSSTC, NSF Cybertraining Grant #1829740, the Brinson Foundation, and the Moore Foundation; his participation in the program has benefited this work. G. L., P. C. and M. P. were supported by a research grant (19054) from VILLUM FONDEN.

This work made use of data from the GROWTH-India Telescope (GIT) set up by the Indian Institute of Astrophysics (IIA) and the Indian Institute of Technology Bombay (IITB). It is located at the Indian Astronomical Observatory (Hanle), operated by IIA. We acknowledge funding by the IITB alumni batch of 1994, which partially supports operations of the telescope. Telescope technical details are available at `https://sites.google.com/view/growthindia/`.

Based on observations made with the Nordic Optical Telescope, owned in collaboration by the University of Turku and Aarhus University, and operated jointly by Aarhus University, the University of Turku and the University of Oslo, representing Denmark, Finland and Norway, the University of Iceland and Stockholm University at the Observatorio del Roque de los Muchachos, La Palma, Spain, of the Instituto de Astrofisica de Canarias.

The Liverpool Telescope is operated on the island of La Palma by Liverpool John Moores University in the Spanish Observatorio del Roque de los Muchachos of the Instituto de Astrofisica de Canarias with financial support from the UK Science and Technology Facilities Council.

The James Clerk Maxwell Telescope is operated by the East Asian Observatory on behalf of The National Astronomical Observatory of Japan; Academia Sinica Institute of Astronomy and Astrophysics; the Korea Astronomy and Space Science Institute; the National Astronomical Research Institute of Thailand; Center for Astronomical Mega-Science (as well as the National Key R&D Program of China with No. 2017YFA0402700). Additional funding support is provided by the Science and Technology Facilities Council of the United Kingdom and participating universities and organizations in the United Kingdom and Canada. Additional funds for the construction of SCUBA-2 were provided by the Canada Foundation for Innovation. The JCMT data reported here were obtained under project M22AP030 (principal investigator D.A.P.). We thank Jasmin Silva, Alexis-Ann Acohido, Harold Pena, and the JCMT staff for the prompt support of these observations. The `Starlink` software is currently supported by the East Asian Observatory.

Competing Interests The authors declare no competing interests.

Contributions IA and MWC were the primary authors of the manuscript. ... All authors contributed to edits to the manuscript.

Correspondence Correspondence and requests for materials should be addressed to Igor Andreoni (email: andreoni@umd.edu) and Michael Coughlin (email: cough052@umn.edu).

Methods

1 Section 1 of methods

2 Data Availability

The data that support the plots within this paper and other findings of this study are available from the corresponding author upon reasonable request.

3 Code Availability

Upon request, the corresponding author will provide code (primarily in python) used to produce the figures.

Supplementary Information

4 Observational details

Identification In recent years, transformative network growth of astronomy facilities and their associated data sets have required a revolution in the data science principles applied to facilitate discovery. For example, LIGO, Virgo, and KAGRA for gravitational waves, IceCube and ANTARES for neutrinos, and ZTF and forthcoming Vera C. Rubin Observatory are transforming astrophysics with detections of never-before-seen phenomena. However, the relative rarity of these events, i.e. the multi-messenger detection of GW170817 remains a once per decade type event, means that rapid improvements in capturing and correlating these data sets using data science principles is required.

For optical astronomy in particular, the advent of surveys such as ZTF requires techniques developed for, in real time, parsing the ~ 1 million alerts produced every night. This real time aspect is essential, as the rapid evolution of the dynamics of the many systems requires that they are discovered and characterized as early as possible, or the opportunity to acquire crucial data is lost. It is these multi-wavelength sources for which follow-up is immediately required, and it is these sources that we target with real-time algorithms such as ZTFReST.

Their discovery and characterization requires a handful of key elements: robust selection criteria to limit the number of objects to only those that are most interesting, rapid photometric and spectroscopic follow-up to uncover their nature, and technical capabilities to perform parameter inference and model selection in near real-time to understand their physics. Unlike in other fields where instruments are regularly upgraded to be more sensitive, it is these technical improvements required to improve upon the base sensitivity of what is possible given the fact that telescope apertures do not become larger and the efficiency of their detectors are not often improved.

AT2022cmc was first discovered by the ZTFReST project[2] which uses ZTF alert packets combined with forced point-spread-function photometry (ForcePhotZTF, cite Yao2019 here or in the addendum) to search for exotic extragalactic transients, including kilonovae from binary neutron star mergers.

Observations and Data Processing

4.0.1 Palomar 48-inch Samuel Oschin Telescope

The ZTF observations ...

4.0.2 Liverpool Telescope

...

4.0.3 Hubble Space Telescope

...

4.0.4 Very Large Array

...

4.0.5 JCMT SCUBA-2 Sub-millimetre Observations

Sub-millimetre observations of AT2022cmc were performed simultaneously at 850 μm (350 GHz) and 450 μm (670 GHz) on two nights using the Submillimetre Common-User Bolometer Array 2 (SCUBA-2) continuum camera[?] on the James Clerk Maxwell Telescope (JCMT) on Mauna Kea, Hawaii. The SCUBA-2 data were analyzed in the standard manner using the 2021A version of `Starlink`[?]; this used Version 1.7.0 of `SMURF`[?] and Version 2.6-12 of `KAPPA`. Observations of the SCUBA-2 calibrator Arp 220 on both nights did not show any anomalous behaviours, so the current standard flux conversion factors were used for the flux normalization [?]. In the SCUBA-2 Dynamic Interactive Map-Maker, the Blank Field map was used for the AT2022cmc observations. The maps were smoothed using a matched filter. The RMS background noise was determined in the central $2'$ of the map with the source excluded.

The SCUBA-2 observations of AT2022cmc are summarized in Table **??**. These expand on the preliminary results given in [[?]]. There was a marginal detection of AT2022cmc at 850 μm on both of the nights. This becomes more significant when all the data are combined, giving an 850 μm flux density of 4.9 ± 1.3 mJy/beam at a mid-point of UT 2022-02-21.510.

AT2022cmc was not detected at 450 μm in the individual night observations or in the combined data; the RMS for the combined data is 10.5 mJy/beam at a mid-point of UT 2022-02-21.510.

4.0.6 GROWTH-India Telescope

The 0.7m GROWTH-India Telescope (GIT) located at the Indian Astronomical Observatory (IAO), Hanle-Ladakh, started observing ZTF22aaajecp at 19:30:26.78 UT on February 15, 2022. The data were acquired in SDSS g', r' and i' bands with multiple 300 sec exposures. Data were downloaded in real time to our data processing unit at IIT Bombay. After a preliminary bias correction & flat fielding and cosmic-rays removal via Astro-SCRAPPY[?] package, all images acquired on same night were stacked making use of SWARP[?]. The pipeline performs point spread function (PSF) fit photometry to obtain the instrumental magnitudes using standard techniques. These magnitudes were calibrated against PanSTARRS DR1 catalogue[?] by correcting for zero points. Reported photometric uncertainties (Table 2) are 1σ values.

4.0.7 Blanco Telescope

We conducted photometric observations of AT2022cmc using the Dark Energy Camera (DECam[42]) optical imager mounted at the prime focus of the Blanco telescope at Cerro Tololo Inter-American Observatory (program ID 2022A-679480, PI Zhang; program ID 2021B-0325, PI Rest). After standard calibration (bias correction, flat-fielding, and WCS) was done by the NSF NOIRLab DECam Community Pipeline[43], difference image photometry was obtained using the `Photpipe` pipeline[44].

4.0.8 Nordic Optical Telescope

We obtained a series of gri photometry with the Alhambra Faint Object Spectrograph and Camera (ALFOSC)[c] on the 2.56 m Nordic Optical Telescope (NOT) at the Observatorio del Roque de los

[c] `http://www.not.iac.es/instruments/alfosc`

Muchachos on La Palma (Spain)[d]. The data were reduced with PyNOT[e] that uses standard routines for imaging data. We used aperture photometry to measure the brightness of the transient. Once an instrumental magnitude was established, it was calibrated against the brightness of several stars from a cross-matched SDSS catalogue.

4.0.9 Palomar 60-inch telescope

Photometry was also obtained on the robotic Palomar 60-inch telescope (P60; [?]) equipped with the Spectral Energy Distribution Machine (SEDM[?]). Photometry was produced with an image-subtraction pipeline[?], with template images from the Sloan Digital Sky Survey (SDSS[?]). This pipeline produces PSF magnitudes, calibrated against SDSS stars in the field.

4.0.10 Palomar 200-inch telescope

We obtained one epoch of observations from the Wide Infrared Camera on the Palomar 200 in telescope. On 2022-03-12 we performed a set of 18 dithered exposures of 45 s each in the J band (1.25μm). We use standard optical reduction techniques in Python to reduce and co-add the images, using 2MASS point source catalog for photometric calibration. We measure aperture photometry using photutils.

4.0.11 Neutron Star Interior Composition Explorer

AT2022cmc has been observed by the Neutron Star Interior Composition Explorer (hereafter NICER[45]) under director's discretionary time (DDT) and ToO programs. The NICER observations will be reported in detail by Pasham et al. in prep. Here we only analyzed the first NICER good time interval (GTI) obtained on 2022 Feburary 16.

We processed the NICER data using `heasoft` v6.29c. We ran `nicerl2` to obtain the cleaned and screened event files. We removed hot detectors. Background was computed using the `nibackgen3C50` tool [46] with hbgcut=0.05 and s0cut=2.0. Response files were generated with

[d]Program ID: 64-501

[e]`https://github.com/jkrogager/PyNOT`

nicerarf and nicerrmf. The spectrum was rebinned using ftgrouppha with grouptype=optmin and groupscale=50. We added systematic errors of 1% using grppha.

The final spectrum has an effective exposure time of 1560 s, and the source is above background at 0.25–8 keV. We fitted the 0.25–8 keV data using tbabs*ztbabs*powerlaw and χ^2-statistics. The Galactic column density $N_{\rm H}$ was fixed at $8.88 \times 10^{19}\,{\rm cm}^{-2}$ [47]. We obtained a good fit with a χ^2/degrees of freedom (χ^2/dof) of 74.91/83. The best-fit power-law index $\Gamma = 1.53 \pm 0.03$, and host galaxy $N_{\rm H} = 1.09^{+0.14}_{-0.13} \times 10^{21}\,{\rm cm}^{-2}$. The observed 0.25–8 keV flux is $(3.29 \pm 0.07) \times 10^{-11}\,{\rm erg\,s^{-1}\,cm^{-2}}$. The inferred absorbed 0.3–10 keV flux is $(3.75 \pm 0.09) \times 10^{-11}\,{\rm erg\,s^{-1}\,cm^{-2}}$. Errors are 90% confidence level for one parameter of interest. The data and best-fit model are shown in the left panel of Fig.2.

4.0.12 Neil Gehrels Swift Observatory

AT2022cmc has been observed by the X-Ray Telescope (XRT[48]) and the Ultra-Violet/Optical Telescope (UVOT[49]) on board Swift under a series of time-of-opportunity (ToO) requests.

All XRT observations were obtained in the photon-counting mode. First, we ran ximage to determine the position of AT2022cmc in each observation. To calculate the background-subtracted count rates, we filtered the cleaned event files using a source region with $r_{\rm src} = 30''$, and eight background regions with $r_{\rm bkg} = 25''$ evenly spaced at $80''$ from AT2022cmc. A log of XRT observations is given in Table 1.

For obsIDs where the XRT net counts are greater than 100, we groupped the spectra to have at least one count per bin, and modeled the 0.3–10 keV data with tbabs*ztbabs*powerlaw. All data were fitted using C-statistics via cstat[50]. We do not find strong evidence of spectral evolution throughout the first seven XRT observations (see Supplementary Information Figure 1). Assuming $\Gamma = 1.53$ and a host galaxy $N_{\rm H} = 1.1 \times 10^{21}\,{\rm cm}^{-2}$, the XRT 0.3–10 keV count rate (in ${\rm count\,s^{-1}}$) to flux (in ${\rm erg\,cm^{-2}\,s^{-1}}$) conversion factor is 4.19×10^{-11}.

The first seven UVOT epochs (obsID 15023001–15023007) were conducted with UBV+All UV filters. Subsequent observations were conducted with U+All UV filters. We measured the UVOT photometry using the uvotsource tool. We used a circular source region with $r_{\rm src} = 5''$, and corrected for the enclosed energy within the aperture. We measured the background using

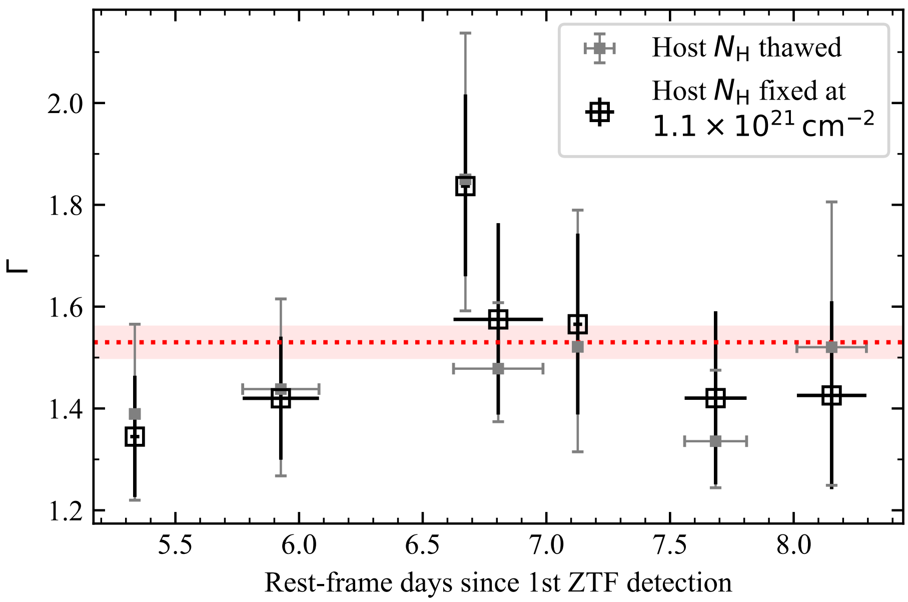

Supplementary Information Figure 1: Evolution of the power-law photon index Γ in the first seven XRT observations. All measurements are consistent with the best-fit Γ in the first NICER observation (§4.0.11), as marked by the horizontal dotted line.

four nearby circular source-free regions with $r_{\rm bkg} = 10''$. The UVOT photometry is presented in Table 2.

4.0.13 ATLAS

We obtained broad-band "orange" and "cyan" light curves from the ATLAS[51] survey. This data is publicly available[f] through the ATLAS Transient Science Server[52]. Detections of AT2022cmc were obtained only in the orange filter.

Very Large Telescope ...

W. M. Keck Observatory ...

Gemini Observatory ...

[f] `https://fallingstar-data.com/forcedphot/`

5 Host galaxy

The field AT2022cmc was observed in u and r with the MegaPrime camera at the 3.58m Canada-French-Hawaii Telescope between 2015 and 2016. We retrieved the science-ready level-3 data from the Canadian Astronomy Data Centre[g]. We used aperture photometry (aperture radius: $1.5 \times$ FWHM of the stellar PSF) to measure the brightness of the host galaxy. Once an instrumental magnitude was established, it was calibrated against the brightness of several stars from a cross-matched SDSS catalogue. The host evaded detection in both bands. Using forced photometry, we measure < 24.19 and < 24.54 mag in u and r band (3σ confidence; not corrected for Milky-Way extinction), respectively.

To put a limit on the host galaxy properties, we model the spectral energy distribution with the software package `Prospector`[h] version 0.3 [53]. `Prospector` uses the `Flexible Stellar Population Synthesis` (`FSPS`) code [54] to generate the underlying physical model and `python-fsps` [55] to interface with `FSPS` in python. The `FSPS` code also accounts for the contribution from the diffuse gas based on the Cloudy models from ref. [56]. Furthermore, we assumed a Chabrier initial mass function [57] and approximated the star formation history (SFH) by a linearly increasing SFH at early times followed by an exponential decline at late times (functional form $t \times \exp\left(-t/\tau\right)$). The model was attenuated with the Calzetti model[58]. The priors were set identical to reference [59].

The fit to the data yields a galaxy mass of $\log M/M_\odot = 8.47^{+1.18}_{-0.74}$, star-formation rate of $9.0^{+62.9}_{-6.1}\ M_\odot\,\mathrm{yr}^{-1}$, and an absolute magnitude of $M_r = -20.4^{+0.6}_{-1.0}$ mag (corrected for Milky Way extinction but not correct for host attenuation). These values should be considered as upper limits.

[g]https://www.cadc-ccda.hia-iha.nrc-cnrc.gc.ca/en/

[h]https://github.com/bd-j/prospector

obsID	Start Date (UT)	δt (days)	Exp. (s)	Net Count Rate ($\mathrm{count\,s^{-1}}$)	Observed Flux ($10^{-13}\,\mathrm{erg\,s^{-1}\,cm^{-2}}$)	Observed Luminosity ($10^{45}\,\mathrm{erg\,s^{-1}}$)
15023001	2022-02-23.11	$+5.32$	2629	0.1552 ± 0.0079	65.03 ± 3.32	52.57 ± 2.69
15023002	2022-02-24.10	$+5.77$	3096	0.1327 ± 0.0078	55.59 ± 3.27	44.94 ± 2.64
15023003	2022-02-25.97	$+6.62$	2737	0.0640 ± 0.0056	26.80 ± 2.33	21.67 ± 1.89
15023004	2022-02-26.04	$+6.65$	2829	0.0640 ± 0.0056	26.80 ± 2.33	21.67 ± 1.89
15023005	2022-02-27.04	$+7.11$	2599	0.0791 ± 0.0057	33.15 ± 2.41	26.80 ± 1.95
15023006	2022-02-28.02	$+7.56$	2694	0.0799 ± 0.0057	33.46 ± 2.37	27.05 ± 1.92
15023007	2022-03-01.02	$+8.01$	2654	0.0658 ± 0.0052	27.58 ± 2.19	22.30 ± 1.77
15023009	2022-03-07.07	$+10.77$	2634	0.0304 ± 0.0036	12.74 ± 1.51	10.30 ± 1.22
15023010	2022-03-10.30	$+12.25$	2829	0.0165 ± 0.0026	6.89 ± 1.11	5.57 ± 0.89
15023011	2022-03-13.43	$+13.67$	1485	0.0166 ± 0.0037	6.95 ± 1.56	5.62 ± 1.26

Supplementary Information Table 1: **XRT observations of AT2022cmc.** δt is rest-frame days since the first ZTF detection epoch. The count rate, flux, and luminosity are given in observer frame 0.3–10 keV. The uncertainties are represented by the 68% confidence intervals, assuming Poisson symmetrical errors.

Extended Data

References

Supplementary Information Table 2: Infrared/Optical/Ultraviolet Photometry table

Date UT	Phase RF	Filter	Mag	eMag	Instrument
2022-01-21 08:57	-9.6093	ZTF_r	> 19.8	-	ZTF
2022-01-21 09:54	-9.5913	ZTF_g	> 19.7	-	ZTF
2022-02-11 10:42	0.0000	ZTF_r	20.71	0.17	ZTF
2022-02-11 11:08	0.0081	ZTF_g	20.91	0.17	ZTF
2022-02-12 09:58	0.4422	ZTF_r	19.08	0.09	ZTF
2022-02-12 09:59	0.4424	ZTF_r	19.15	0.11	ZTF
2022-02-12 10:21	0.4493	ZTF_i	18.88	0.09	ZTF
2022-02-12 11:27	0.4702	ZTF_g	19.33	0.06	ZTF
2022-02-12 11:57	0.4797	ZTF_r	19.10	0.04	ZTF
2022-02-12 12:03	0.4817	ZTF_g	19.53	0.06	ZTF
2022-02-12 12:34	0.4913	ZTF_r	19.08	0.04	ZTF
2022-02-13 09:47	0.8945	ZTF_r	19.69	0.10	ZTF
2022-02-13 10:20	0.9048	ZTF_g	19.81	0.12	ZTF
2022-02-14 09:36	1.3472	ZTF_r	19.87	0.12	ZTF
2022-02-14 09:39	1.3480	ZTF_r	19.78	0.11	ZTF
2022-02-14 12:50	1.4085	ZTF_g	20.38	0.20	ZTF
2022-02-14 12:52	1.4090	ZTF_g	20.06	0.14	ZTF
2022-02-15 00:52	1.6372	r	20.22	0.14	IOO
2022-02-15 00:55	1.6379	i	20.12	0.16	IOO
2022-02-15 00:57	1.6386	z	19.82	0.14	IOO
2022-02-15 02:13	1.6629	r	20.43	0.08	IOO
2022-02-15 02:18	1.6644	i	20.13	0.09	IOO
2022-02-15 02:23	1.6659	z	19.78	0.10	IOO
2022-02-15 05:54	1.7327	g	20.72	0.18	IOO
2022-02-15 06:00	1.7345	r	20.17	0.10	IOO
2022-02-15 06:05	1.7363	i	20.16	0.09	IOO
2022-02-15 06:11	1.7381	z	19.91	0.12	IOO
2022-02-15 07:53	1.7704	ZTF_i	> 19.4	-	ZTF
2022-02-15 08:43	1.7863	g	20.57	0.21	DECam
2022-02-15 08:43	1.7864	ZTF_g	> 19.4	-	ZTF
2022-02-15 08:44	1.7866	r	20.59	0.13	DECam
2022-02-15 08:45	1.7869	i	20.13	0.20	DECam
2022-02-15 09:50	1.8076	ZTF_r	> 19.7	-	ZTF
2022-02-15 20:11	2.0043	r	20.67	0.09	GITCamera
2022-02-15 23:43	2.0714	r	20.68	0.08	GITCamera
2022-02-16 09:01	2.2479	i	21.24	0.28	DECam